PAPER

Check for updates

Effects of crowding on the diffusivity of membrane adhered particles

Paige Liu (iD) and Peter J. Beltramo (iD) *

The lateral diffusion of cell membrane inclusions, such as integral membrane proteins and bound receptors, drives critical biological processes, including the formation of complexes, cell–cell signaling, and membrane trafficking. These diffusive processes are complicated by how concentrated, or ''crowded'', the inclusions are, which can occupy between 30–50% of the area fraction of the membrane. In this work, we elucidate the effects of increasing concentration of model membrane inclusions in a free-standing artificial cell membrane on inclusion diffusivity and the apparent viscosity of the membrane. By multiple particle tracking of fluorescent microparticles covalently tethered to the bilayer, we show the transition from expected Brownian dynamics, which accurately measure the membrane viscosity, to subdiffusive behavior with decreased diffusion coefficient as the particle area fraction increases from 1% to around 30%, approaching physiological levels of crowding. At high crowding, the onset of non-Gaussian behavior is observed. Using hydrodynamic models relating the 2D diffusion coefficient to the viscosity of a membrane, we determine the apparent viscosity of the bilayer from the particle diffusivity and show an increase in the apparent membrane viscosity with increasing particle area fraction. However, the scaling of this increase is in contrast with the behavior of monolayer inclusion diffusion and bulk suspension rheology. These results demonstrate that physiological levels of model membrane crowding nontrivially alter the dynamics and apparent viscosity of the system, which has implications for understanding membrane protein interactions and particle-membrane transport processes.

1 Introduction

Biological membranes have a critical function in nature, acting as the outer boundary of a cell, as well as the barrier that compartmentalizes organelles. The membrane backbone is the phospholipid bilayer, a pseudo two-dimensional interface which is flexible, tensionable, and fluid in nature to allow for the lateral diffusion of membrane components, including peripheral and integral membrane proteins, which can comprise up to 50% by mass (or area) of the membrane.[1–3] The mobility of these inclusions is critical to many of the structure, signaling, and transport functions of the cellular membrane.[4] For example, the reduced lateral diffusivity of different receptors allows for them to cross-link in order to form a signaling complex.[5] Concentrated quantities of intrinsically disordered peripheral membrane proteins cause steric pressure on the membrane, allowing membrane fission to occur more readily.[6,7] Membrane undulations, tension and bending rigidity both impact the behavior of and are affected by the presence of ion channels, as has been shown theoretically,[3] by molecular dynamics simulations,[8] and experimentally.[9]

Department of Chemical Engineering, University of Massachusetts Amherst, Amherst, MA 01003, USA. E-mail: pbeltramo@umass.edu

The crowded nature of biological cell membranes induces complex anomalous dynamics of proteins and inclusion molecules, with subdiffusion observed in experiments on living cells, experimental artificial bilayer studies, and simulations of the cell membrane. For example, fluorescence correlation spectroscopy (FCS) was used to study the diffusion of Golgi resident membrane proteins in HeLa cells, finding lower than expected diffusion coefficients and subdiffusion.[10] Manzo and Garcia-Parajo[11] showed, with a combination of simulations and single particle tracking measurements of the diffusion of transmembrane proteins, subdiffusion arising from temporal or spatial heterogeneity within the plasma membrane. In addition to protein inclusion crowding being a source of anomalous dynamics, bilayer interactions with the cytoskeletal environment also influence the dynamics within cell membranes. For example, clathrin interacts with specific lipids and proteins to form a clathrin coated pit to initialize endocytosis,[12] and remodeling of the cortical actin network causes non-Gaussian dynamics of acetylcholine receptors.[13] A combination of macromolecular crowding and transient compartmentalization/binding to the actin cytoskeleton causes anomalous dynamics of the Kv2.1 potassium ion channel.[14,15] It would be of value to divorce the effects of protein crowding from native cell environments, which have complicating factors

such as the cytoskeleton and immobile barriers to diffusion, in order to elucidate the effect of crowding in a simplified model membrane system.

Simulations have revealed several contributing factors underlying these anomalous membrane dynamics. For example, it was shown that, depending on protein size, subdiffusive dynamics arise as membrane crowding increases.[16] Non-Gaussian behavior was observed in coarse grained and stochastic modeling of protein crowding in a DPPC lipid bilayer and attributed to spatiotemporal heterogeneity in lipid diffusion.[17] Specific lipid–protein interactions also can contribute to subdiffusive translational and rotational dynamics of proteins, such as the interaction between pleckstrin homology domains and phosphatidyl–inositol phosphate lipids revealed by multiscale molecular dynamics simulations.[18,19]

A number of different model membrane systems have been leveraged to investigate the dynamics of membrane inclusions in order to understand the fundamental underpinnings of these biological processes, from the dilute to crowded regime. Peters and Cherry[20] measured bacteriorhodopsin and lipid diffusion simultaneously in multilamellar vesicles, which was one of the first experiments to show that steric effects due to crowding were likely to alter membrane dynamics. Studies using supported lipid bilayers (SLBs) have indicated a decrease in the diffusivity of membrane inclusions with increasing crowding as well as the observation of anomalous diffusion.[21–23] However, it remains unclear how crowding would impact the diffusivity of membrane inclusions in free-standing model membranes, where interactions between the substrate and the lipid bilayer would not affect inclusion diffusivity. Such systems also confer the advantage of being able to manipulate the bending rigidity and tension of the membrane. Studies in this regard have been done measuring changes in the diffusion coefficient of proteins against their concentration in GUVs, with the highest protein concentration measured to be $\approx 10^3$ proteins per μm^2 (less than 10% by area).[24] However, physiological levels of inclusion crowding (30–50% by area), either using membrane proteins or model inclusion systems, have not been investigated in the context of a free-standing model membrane.

In the dilute limit, the diffusion of peptides and proteins reconstituted in black lipid membranes (BLMs)[25] and giant unilamellar vesicles (GUVs)[26] was found to be well-represented by the hydrodynamic continuum theory developed by Saffman and Delbrück,[27] which gives Λ_T, the translational drag coefficient, as

$$\Lambda_T = \frac{4\pi\eta_m}{\ln(2\varepsilon^{-1}) - \gamma} \tag{1}$$

where η_m is the 2D membrane viscosity, $\gamma = 0.5772$ is Euler's constant, and $\varepsilon = 2\eta a/\eta_m$ is a dimensionless length scale relating η_m to a (the inclusion radius) and η (the bulk viscosity of the fluid surrounding the bilayer interface).[27] The translational drag coefficient, and subsequently the membrane viscosity, can then be found from the diffusion coefficient by the Einstein relation, $D_T = k_B T/(\Lambda_T)$, where k_B is the Boltzmann constant and T is the temperature. We note that the derivation of eqn (1) is in the limit of infinite dilution (one inclusion in an infinite area bilayer) and predicts a logarithmic dependence of diffusivity with inclusion radius. However, simulations have shown that, as crowding increases, the diffusivity of inclusions scales with a power-law dependence.[16]

Colloidal particles strongly adhered to lipid bilayers via avidin coated particles binding to biotinylated lipids have been used in conjunction with eqn (1) in order to measure the viscosity of lipid bilayers in the dilute limit. Hormel et al.[28] used dicolloidal probes with two 200 nm diameter lobes to measure simultaneous translational and rotational diffusion, demonstrating an increase in membrane viscosity with increasing concentrations of the vesicle tracking protein Sar1p. Later, the same group used 3 μm by 1 μm polystyrene ellipsoids to show consistent measurement of membrane viscosity between tracking membrane-anchored particles and phase-separated lipid domains.[29] Collectively, these results show the utility of using avidin–biotin linkages between microparticles and membranes in order to accurately determine membrane viscosity in the dilute limit, but the impact on increasing colloidal particle area fraction on the dynamics and apparent viscosity of the membrane has not been explored.

The crowding of colloidal particles on free-standing, flexible, interface such as a phospholipid bilayer is also an interesting problem from a hydrodynamic and thin film mechanics standpoint. The rheology of bulk particle suspensions has been thoroughly investigated both in experimental and theoretical terms and has been well characterized with respect to changes in the particle volume fraction. A dilute suspension of particles is known to have a viscosity which scales against the particle volume fraction, ϕ, according to the Einstein relation $\eta = \mu\left(1 + \frac{5}{2}\phi\right)$.[30] As random close packing is approached, the effective viscosity of the suspension scales as $1 - (\phi/\phi_m)^{-2}$, where ϕ_m is the volume fraction for random close packing.[31] However, an analogous scaling is not well developed for colloidal crowding at a static or flexible two-dimensional interface. At a fluid interface, inter-particle forces are complicated by the hydrodynamic contribution of the surrounding fluid,[32] therefore it has been an on going challenge to determine what is dictating changes in 2D fluidity with crowding.[33]

In a lipid monolayer system, 2D crowding was studied by controlling the area fraction of solid domains diffusing within a continuous fluid phase.[34] The surface viscosity of the continuous phase was found to scale with the increasing area fraction of the solid domains in a power law relationship, and this scaling was found to be consistent with that of 3D suspensions. Investigating these scaling effects on a flexible interface where the material properties (bending rigidity, tension) of the interface can be controlled, such as in a lipid bilayer membrane, in order to understand dynamic biological processes is the goal of this and future work.

In this study, we use neutravidin functionalized microspheres tethered to a biotinylated lipid bilayer to probe the effects of increasing particle concentration on the apparent rheology of the bilayer–particle system. Particle dynamics are

monitored on a large area model biomembrane (LAMB), a planar, free-standing membrane platform, affording ease of imaging for particle tracking and crowding studies. 1,2-dioleoyl-sn-glycero-3-phosphocholine (DOPC) is used as the basis for the model bilayer since it has been used in several studies of bilayer viscosity, allowing the validation of membrane viscosity in the dilute limit. We then show the impact of increasing particle crowding on membrane dynamics, revealing decreases in diffusion coefficient and subdiffusion. Finally, we relate these changes in diffusivity to changes in the apparent viscosity of the 2D system, demonstrating scaling behavior which contrasts that of bulk suspensions and monolayer interfaces.

2 Methods

2.1 Materials

The lipids DOPC and 1,2-dioleoyl-sn-glycerol-3-phospho-ethanolamine-N-(cap biotinyl) (DOPE-cb) were obtained from Avanti Polar Lipids (Alabaster, AL). HPLC-grade chloroform, n-hexadecane, otadecyltrichlorosilane (OTS), sodium chloride (NaCl), sodium bicarbonate (NaHCO$_3$), and calcium chloride (CaCl$_2$) were purchased from Thermo Fisher Scientific (Waltham, MA). Before use, the hexadecane is filtered twice through a 0.2 μm aluminum oxide mesh (Sigma Aldrich). Fluorescent and non-fluorescent neutravidin functionalized 1 μm diameter microspheres were from Molecular Probes (Eugene, OR). All aqueous solutions were prepared using ultra-pure water filtered using a reverse osmosis system from Millipore (Billerica, MA) and filtered using a 0.2 μm pore filter. The glass microfluidic "bikewheel" chip was custom fabricated by Micronit (Enschede, the Netherlands), and the sample holder was 3D printed using VeroWhite from Stratasys (Eden Prairie, MN). The chip has channels leading to a "bikewheel" with 24 spokes leading into an open aperture which is 0.9 mm in diameter and is installed in an aluminum holder leading to a capillary tube. To commission the microfluidic chip for making a bilayer, the chip is cleaned in a concentrated solution of NaOH in ethanol, then functionalized in a solution of OTS in hexadecane to make the surface slightly hydrophobic.

2.2 Bilayer fabrication

Bilayers are formed on the LAMB platform as previously described.[35–39] Briefly, DOPC and DOPE-cb are diluted in chloroform to form stock solutions. These stock solutions are then combined in a 7 mL scintillation vial according to a target molar composition, typically 99 to 1 DOPC to DOPE-cb. The combined solution is then dried under nitrogen to remove excess chloroform then fully dried overnight under vacuum at ≤20 millibar. The dried lipids are then resuspended in hexadecane at a concentration of 2.5 mg mL^{-1}, and the resulting lipid–oil mixture is sonicated for at least 2 hours before use in an experiment.

To form the bilayer, the microfluidic chip is first loaded with the lipid–oil mixture. The chip is then loaded into a sample holder with chambers for aqueous buffer and a temperature control system to keep the sample at 25 °C. The capillary is connected to a pressure control system (ElveFlow), which is used to control the drainage of the lipid–oil film formed in the center of the aperture and the area of the subsequent bilayer. The pressure on the chip is first increased quickly to form a thick film across the aperture, then the pressure is slowly decreased to allow the film to thin. When the film has thinned sufficiently, a lipid bilayer nucleates and then populates an area that is kept constant at around 0.5 mm^2 using the pressure control system.

2.3 Particle addition and imaging

Fluorescent 1 μm diameter neutravidin functionalized latex particles, which strongly adhere to the biotinylated lipids in the bilayer, are used as probes to measure membrane fluidity (Fig. 1A). Particle crowding is controlled by the amount of particles added and allowed to settle on the bilayer, or by changing bilayer area. At higher fluorescent particle concentrations, it becomes difficult to resolve individual particles (Fig. 1B). To reduce the amount of fluorescent noise and overcome this limitation, fluorescent particles are combined with unlabeled particles which have the same surface functionalization and diameter at a 1:19 number ratio. This allows for high area fractions to be imaged without a loss in individual particle resolution (Fig. 1C). The particles are diluted from their stock suspensions and then added to the bilayer by pipetting them in 2 μL aliquots into the top chamber of the sample cell. After allowing 15–30 minutes for the particles to settle, fluorescence images of the bilayer–particle system are taken at 20 FPS under 40× zoom (Nikon Ti-2e). In a given experiment, multiple videos are taken to be analyzed, with at least 200 particles in focus for each video.

2.4 Particle tracking and analysis

Particle location and tracking was done using a brightness weighted centroid algorithm.[40] After initially filtering by intensity, the particle count from the particle tracking software was used to estimate a particle area fraction, A, by:

$$A = m \times A_p \qquad (2)$$

where m is the particle count and A_p is the projected area per particle. We calculate A_p according to the stock radius of the particles used. When using a mixture of fluorescent and unlabeled particles, $(m \times A_p)$ is multiplied by the ratio of bright to dark particles to obtain the final particle area fraction.

After the particle tracks were further filtered by size and eccentricity, the mean squared displacements (MSDs) of the individual particle tracks were calculated. The individual MSDs were then averaged together to obtain an ensemble MSD. The ensemble MSD can be used to fit an anomalous diffusion descriptor, which is defined by a power law according to:

$$\langle \Delta r^2 \rangle = 4Dt^n \qquad (3)$$

where $\langle \Delta r^2 \rangle$ is average particle displacement in two dimensions, D is the diffusion coefficient, t is the lag time, and n is the scaling exponent of the MSD.
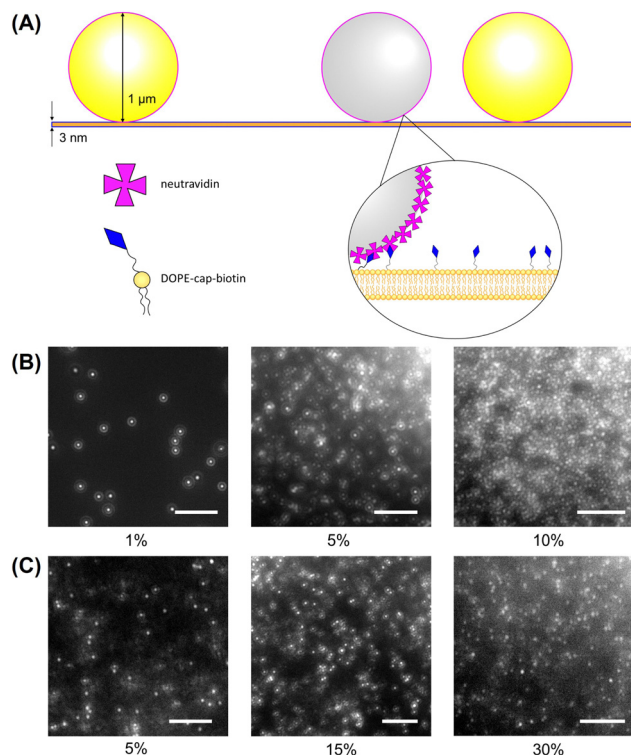
Fig. 1 (A) Schematic of the experimental setup showing the linkage of neutravidin functionalized microspheres with biotinylated lipids on a free-standing phopsholipid membrane. To increase ease of particle tracking, fluorescent particles are mixed with unlabeled particles with the same size and surface functionalization. (B) As the particle area fraction on the bilayer increases from the dilute range (<1%) to quantities approaching physio-logical crowding (10%), the increase in particle density is apparent optically. (C) To mitigate the noise introduced by overlapping fluorescence signals, mixed fluorescent and unlabeled particles can be used to increase signal-to-noise even while higher levels of crowding (30%) are achieved. The scale bar for all images is 20 μm.

As expanded upon below, a decreasing diffusion coefficient and the appearance of subdiffusive dynamics are observed with increasing particle area fraction. We note that erroneous identification of subdiffusion has been observed in single-particle tracking experiments.[41] However, robust criteria for verifying the presence of either subdiffusive, diffusive, or super-diffusive dynamics have been developed by analysis of the power spectral density of the trajectories.[42] We have applied these criteria to our trajectories to validate that the observation of subdiffusion is independent of any remnant static or dynamic localization errors. Related machine learning models are also under development in order to both identify different modes of diffusion and extract further insight into the observed dynamics.[43]

3 Results and discussion

3.1 Determination of dilute membrane viscosity

In order to assess how the fluidity of the bilayer changes with crowding, we first use experiments in the dilute regime to benchmark measurements of membrane viscosity determined

using different hydrodynamic models against literature values. We start by evaluating the efficacy of the Saffman–Delbrück model within our system.[27] At dilute area fractions ($A \approx 0.01$), we observe that particle trajectories on a 99/1 DOPC/DOPE-cb bilayer are unhindered, and their MSDs fit a classical Brownian model, in which the exponent of the lag time is $n = 1$ (Fig. 2A). The diffusion coefficient at low concentrations was found to be 0.39 μm^2 s^{-1}. Comparatively, the diffusion coefficient for a 1 μm^2 s^{-1} latex particle in a bulk aqueous solution at the same temperature would be 0.49 μm^2 s^{-1}. As a control, we measured the diffusion of particles that had settled on the surface of a DOPC membrane with no biotinylated lipids and found that their diffusion coefficient was close to the expected diffusion coefficient of these particles in bulk, so the reduced diffusion coefficient with biotin–streptavidin linkages present indicates adhesion to the membrane. Based on an estimated inclusion radius of 100 nm, a membrane thickness of 3 nm measured in previous experiments,[37] and an expected membrane viscosity of $\mathcal{O}(1)$ nPa s m, we expect the dimensionless parameter ε to be order 1 (see eqn (1)). In this range, the Saffman–Delbrück
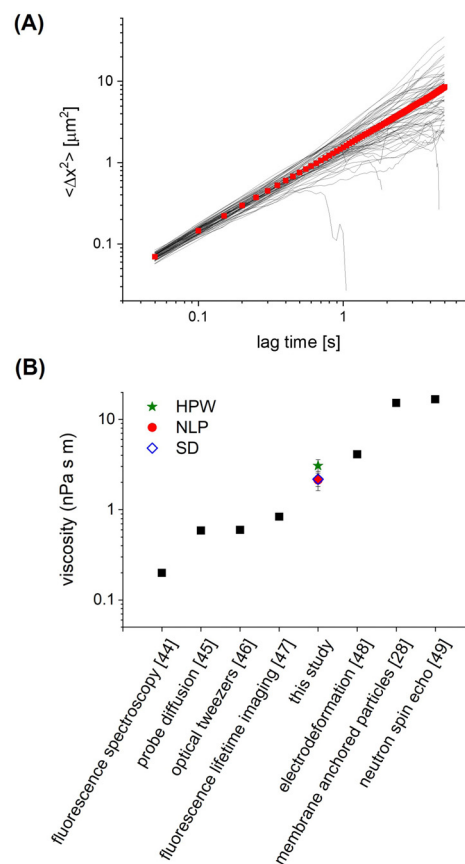
Fig. 2 (A) Ensemble MSD (red) and individual particle tracks (grey) for dilute ($A = 0.01$) 1 μm diameter particles on a 99/1 DOPC/DOPE-cb bilayer. (B) The membrane viscosity calculated from the diffusion coefficient using different models compares well to the range of viscosity values found in literature for DOPC. Example viscosities shown are measured using fluorescence spectroscopy,[44] probe diffusion,[45] optical tweezers,[46] fluorescence lifetime imaging,[47] electrodeformation,[48] membrane anchored particles,[28] and neutron spin echo.[49]

model is no longer strictly valid, but if applied, yields η_m = 2.2 nPa s m.

Extended approaches have been developed to account for larger values of ε. By accounting for the flow field around a membrane inclusion, Hughes, Pailthorpe, and White (HPW) extended the asymptotic solutions of the SD model for arbitrary values of ε, in which the translational drag on the inclusion scales by $f_t \propto \eta_m h \varepsilon$.[50] Petrov *et al.* developed empirical solutions to the HPW hydrodynamic model which have been validated for $10^{-3} < \varepsilon < 10^3$:[51]

$$f_t = 4\pi\eta_m h\left\{\ln\frac{2}{\varepsilon} - \gamma + \frac{4\varepsilon}{\pi} - \frac{\varepsilon^2}{2}\ln\frac{2}{\varepsilon}\right\}^{-1}$$
$$\times \left\{1 - \frac{\varepsilon^3}{\pi}\ln\frac{2}{\varepsilon} + \beta(\varepsilon, b_{t1}, b_{t2}, c_{t1}, c_{t2})\right\} \quad (4)$$

where β is a bridging function, and b_{t1}, b_{t2}, c_{t1}, and c_{t2} are constants. Using these solutions, an apparent viscosity of 3.1 nPa s m is found in the dilute case.

We additionally consider the size and protrusion effects of our probe particle against the membrane hydrodynamic length scale, $l_m = \eta_m/\eta$, intrinsic to the SD and HPW models. From our initial dilute viscosity result, we find $l_m \approx 17a$. At this length scale, in which l_m is not grossly greater than a, dissipation of momentum caused by the inclusion in the bulk fluid should be considered. The effect of locally induced curvature on the effective mobility of a membrane inclusion was incorporated into a model developed by Naji, Levine, and Pincus (NLP):[52]

$$\mu_{\text{eff}} = \frac{\mu_{\text{membrane}}}{1 + c\eta a\mu_{\text{membrane}}} \quad (5)$$

where μ_{eff} is the effective mobility and c is a constant that roughly correlates to the ratio of the volume of bulk fluid displaced by the membrane deformation to a^3. The effective use of the NLP as a hydrodynamic model has been demonstrated by Hormel and Parasarathy in an experiment using dicolloidal probes on a GUV.[28] Using $c^{1/3} = 3$, as measured by Hormel *et al.*,[28] we find a dilute apparent viscosity of 2.1 nPa s m.

We validate our approach by comparing to DOPC viscosity measurements previously reported in the literature. Despite the varied assumptions and considerations in each model, all result in values for the DOPC membrane viscosity that are well within the range of DOPC bilayer viscosities reported in literature (Fig. 2B),[28,44–49] with the caveat that these literature values span two orders of magnitude. Our results are most closely aligned with the viscosity of 4.11 nPa s m measured by electro-deformation of a giant unilamellar vesicle.[48] Since the NLP model relaxes the inherent assumptions of the simpler models to more closely accommodate the nature of this experimental system, it will be used in the analysis of crowded membrane dynamics that follows. We note that the choice of inclusion radius in the range of 50–150 nm for our 500 nm radius particle alters the membrane viscosity by 25–30%, still well within the range determined *via* other methods. More important than the exact value of membrane viscosity, however, is the dependence of viscosity with crowding, which does not appreciably change

with choice of inclusion radius. This is discussed in Section 3.3. In Section 3.2, we further analyze the dynamics and statistics of microparticle diffusion with increased crowding without any assumptions.

3.2 2D particle crowding effects

Over a series of experiments, particle concentrations ranging from dilute coverage ($A < 0.01$) to coverage approaching physiological levels of crowding ($A \approx 0.3$) on a DOPC bilayer with 1 mol% biotinylated lipids were measured. As a control, experiments in the dilute regime were performed on lipid bilayers without biotinylated lipids. As the particle area fraction increases, particle diffusion becomes attenuated, as shown in Fig. 3(A) and (B). Fitting this data to eqn (3) reveals that particle tethering causes a significant decrease in diffusion coefficient, from 0.48 to 0.39 µm² s⁻¹, in the dilute regime. This indicates that the particles, which have over an order of magnitude smaller diffusion coefficient than the lipids ($D_{\text{lipid}} \sim 10$ µm² s⁻¹) are in effect immobilizing the lipids and restricting their diffusion to the tethered region, which in turn attenuates the diffusion of the microparticle (Fig. 3C). As the particle concentration increases, the diffusion coefficient decreases to around 0.3 µm² s⁻¹ at high crowding (30% area fraction, Fig. 3C), with a concurrent decrease in n (Fig. 3D). The source of this subdiffusion may be due to a number of factors, which we discuss through the rest of this section.

It is most straightforward to explain the decrease in diffusivity by steric effects, which are represented in the Boltzmann lattice model:

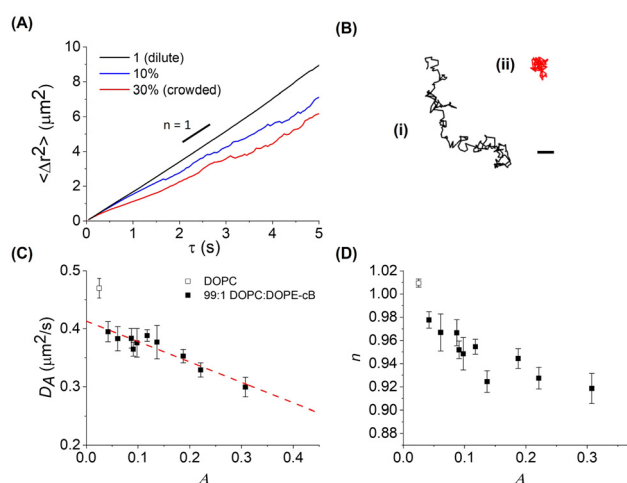$$\frac{D}{D_0} = \alpha(1 - \beta A) \quad (6)$$

Fig. 3 (A) Ensemble MSDs with increasing particle area fraction on a 99 : 1 DOPC : DOPE-cB bilayer. (B) Example particle tracks from a more dilute system (i) compared to a particle track from a high area fraction experiment (ii) (scale bar = 1 µm). (C) The diffusion coefficient of the particles is shown to decrease with increasing particle area fraction, A. Line is a linear fit to the data as described in the text. (D) The exponent of the power law decreases from 1 as particle fraction increases, indicating subdiffusive behavior.

Here, D_0 is the particle diffusivity under dilute conditions, A is the particle area fraction, and α and β are constants. From a least squares regression, we find α = 1.01 and β = 0.79. Measurements of the two-dimensional diffusivity of PMMA spheres of a similar size at a decalin–water interface found α = 0.97 and β = 1.4.[33] We find that the values found for α are comparable while a discrepancy arises between the two values of β. The difference in the two values might arise from the stronger difference in viscosities of the membrane and surrounding aqueous solution as opposed to the oil–water interface. We should also consider the covalent tethering of our particles to the membrane interface, while spheres in the oil–water system are not specifically adhered to the interface, but pinned by capillary forces. While the interfacial viscosity and surface tension of the oil–water interface can be adjusted *via* the addition of surfactant, here the interface is characterized by a bending rigidity, in addition to membrane viscosity and tension.

In bulk suspensions, it has been shown that $D_S^S/D_0 = 1 - \beta_{3D}\phi$, where D_S^S is the short time self-diffusion coefficient, ϕ is the volume fraction of particles, and β_{3D} is the equivalent scaling coefficient for a bulk system. Using diffusing wave spectroscopy, β_{3D} was measured to be approximately 1.86.[53] This β_{3D} was determined to be independent of particle size[53,54] and slightly lower than the theoretically predicted value of 5/2.[30] From these results, it is apparent that in moving from bulk suspensions to monolayers to bilayers, the α term remains constant while β steadily decreases. In going from 3D to 2D diffusion, steric effects have a reduced impact, while when moving from monolayers to bilayers, the ability of the free-standing membrane to be flexible likely further attenuates steric interactions. We expect the particle size dependence of the particle diffusivity scaling observed in monolayers to also manifest in particles tethered to bilayers and are interested in exploring this facet in the future.

The decrease in diffusion coefficient coincides with a decrease of the exponent of the power law descriptor, n, from 1 to 0.9 at higher particle area fractions, indicating subdiffusion of particles caused by interparticle crowding (Fig. 3D).

Similar anomalous diffusion behavior has been reported on SLB systems as well as in simulations.[21,22,55,56] Interestingly, measurements of particle trajectories on supported bilayer systems find evidence of subdiffusion even when membrane inclusions are dilute. We postulate that this may arise from additional interactions between the inclusion, the membrane, and the SLB substrate whereas the model membrane in this work is free-standing, causing subdiffusion to only appear at higher area fractions.

In order to understand the underlying mechanism of the observed subdiffusion, we analyze the onset of non-Gaussian behavior as crowding increases. As a first check, we compare the Van Hove self correlation function of untethered dilute particles ($A = 0.01$, DOPC, dilute), tethered dilute particles ($A = 0.01$, DOPC/DOPE-cB, dilute), and tethered crowded particles ($A = 0.30$, DOPC/DOPE-cB, crowded) at 800 ms lag times. The Van Hove function gives the probability that particle j will move in the vicinity r within time t:

$$G_s(\Delta r, t) = \langle \delta(r - \Delta r_j) \rangle \qquad (7)$$

If the particle displacement is expected to be Gaussian, the Van Hove function can be written as:

$$G_s(\Delta r, t) = \left(\frac{2\pi}{\mathbb{D}}\langle \Delta r^2(t)\rangle\right)^{-\frac{\mathbb{D}}{2}} \exp\left(-\frac{\mathbb{D}\Delta r^2}{2\langle \Delta r^2(t)\rangle}\right) \qquad (8)$$

where $\mathbb{D}$ is the number of dimensions. We see that the displacement of dilute particles at 800 ms follows Gaussian behavior, but the displacements of the particles in the crowded, tethered system have a narrower distribution (Fig. 4A). Complementary to the Van Hove correlation, the excess kurtosis can be calculated as a measure of deviation from Gaussianity of the particle movement:

$$K_\alpha = \frac{\left\langle [\Delta r_\alpha(t) - \langle \Delta r_\alpha(t)\rangle]^4 \right\rangle}{3\left\langle [\Delta r_\alpha(t) - \langle \Delta r_\alpha(t)\rangle]^2 \right\rangle^2} - 1 \qquad (9)$$

We find that in the three cases, the excess kurtosis becomes negative at a lag time of around 1, indicating platykurtotic behavior (Fig. 4B). The test statistic Z_{K_α} is used to determine
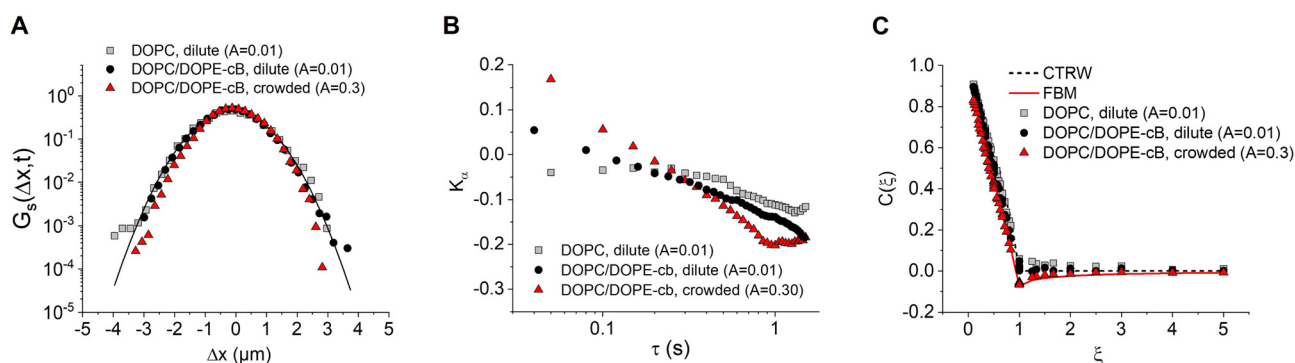
Fig. 4 (A) The Van Hove Correlations for three cases of particles on a lipid bilayer (DOPC, dilute; DOPC/DOPE-cB, dilute; DOPC/DOPE-cB, crowded) demonstrate non-Gaussian behavior for the crowded case. The solid black line is for a Gaussian distribution. (B) The excess kurtosis becomes more significantly negative for a biotinylated bilayer compared to one with no biotin. The approach to negative kurtosis is steeper for a crowded biotinylated bilayer than one with dilute particle coverage. (C) The VACF of the particles becomes negative for a crowded, biotinylated bilayer, indicating anti-persistent motion.

whether or not the deviation of K_α from 0 is signficant. It is defined as $Z_{K_\alpha} = K_\alpha/\sigma_{K_\alpha}$, where:

$$\sigma_{K_\alpha} = \sqrt{\frac{24N(N-1)^2}{(N-3)(N-2)(N+3)(N+5)}} \qquad (10)$$

From this, we find that cutoff for a significantly non-zero value of K_α is -0.1. For our data, this shows that the diffusion of untethered particles remains Gaussian, as expected, but the deviation from Gaussianity for particles both in the dilute and crowded ranges is observed.

Lastly, we consider models that might be used to describe the onset of non-Gaussian, subdiffusive behavior with 2D crowding. Anomalous diffusion models have been developed to describe diffusive dynamics in the crowded cell environment. Three such models commonly applied to cell dynamics are the continuous time random walk (CTRW), the obstructed diffusion model (OD), and the fractional Langevin equation (FLE). CTRW is characterized by random jump lengths following a power law distribution and has been used to describe motion in systems such as colloidal tracers moving in an actin network.[57] In contrast, FLE and its subcase, fractional Brownian motion (FBM), are self-similar processes which have been used to describe such systems as the anomalous diffusion of lipids in a cholesterol doped environment, the diffusion of membrane-binding protein domains, and subdiffusion in the cytoplasm.[19,58,59] It should be noted that recent work has suggested that none of these models completely describe anomalous diffusion with respect to crowding, and a hybrid model may need to developed for a complete description.[17] To see how our data fits these models, we test for the onset of anti-persistence in the particle motion as crowding increases with the velocity autocorrelation function (VACF):[59]

$$C(\tau) = \left\langle \frac{\langle v(t)v(t+\tau) \rangle_t}{\langle v(t)^2 \rangle_2} \right\rangle_E \qquad (11)$$

where the instantaneous velocity is defined as $v(t) = [r(t+\delta t) - r(t)]/\delta t$ taken within integer multiples of the experimental time step so that $\delta t = n\Delta t$. The lag time can be additionally rescaled as $\tau = k\Delta t$, which allows for a dimensionless time to be defined as $\xi = \tau/\delta t = k/n$. We plot the VACF for the same three

cases we compared for excess kurtosis in Fig. 4C, where it is shown that a negative VACF at $\xi = 1$, indicating antipersistent behavior, is evident for the case of crowded particles on a biotinylated bilayer. Fitting the data to the CTRW and FBM models shows that in the dilute regime the particle dynamics follow CTRW, while a strong fit to the FBM model suggests an onset of antipersistence in the particle motion in the crowded regime.

We additionally consider the possibility that the lipids themselves become immobilized as biotinylated lipids in the bilayer tether to a large, slower moving particle. Therefore, the decrease in the diffusion coefficient may not simply arise out of crowding but may also be due to particle–bilayer interactions reducing phospholipid mobility within the bilayer. This idea is supported by computational studies which show that membrane proteins form a complex with the lipids surrounding them and that the lipids in this complex diffuse more slowly relative to lipids outside the immediate vicinity of the protein.[60] While this phenomenon has not been studied extensively in lipid–particle systems, viscosities that are higher than would be expected in literature have been measured in a similar system utilizing a two-particle complex as a probe to measure membrane viscosity, which indicates deformation of the membrane and/or immobilization of lipids surrounding those directly adhered to a probe may be affecting the overall membrane viscosity.[28] However, such an effect should impact all experiments, regardless of area fraction.

3.3 Scaling of effective viscosity with crowding

The inclusion crowding and decrease in diffusion coefficient affect the apparent rheology of the membrane–particle system. The bilayer viscosity for the different diffusion coefficients measured with increasing particle coverage is calculated using the NLP model (Fig. 5(A) and (B)). The viscosity of the bilayer increases significantly with increasing particle area fraction, going from 2 to 3.5 nPa s m.

As mentioned earlier, in a bulk 3D suspension of hard spheres in a viscous fluid, it has been shown that the suspension viscosity scales quadratically with volume fraction.[31] Analogous behavior was also observed in a monolayer system
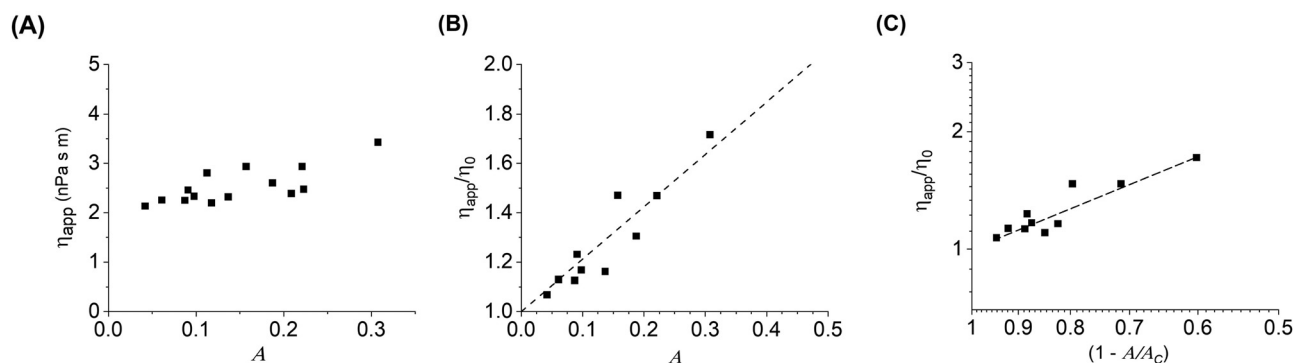

Fig. 5 (A) The apparent viscosity of the bilayer calculated from probe diffusivity increases with increasing area fraction of particles on the bilayer surface. (B) The apparent viscosity scaled by the dilute viscosity, showing a linear increase. (C) The same data plotted against the critical area fraction in analogy to 2D monolayer and 3D suspensions to test a power law behavior.

of highly viscous domains diffusing in a continuous low viscosity matrix, where the viscosity of the entire monolayer system increased as a power law,[34] $\eta_s/\eta_{so} = [1 - A/A_c]^{-2.07}$, where η_s is the measured shear viscosity of the system, η_{so} is the shear viscosity of the continuous lipid matrix, and A_c is the critical inclusion area fraction analogous to the sphere volume fraction at random close packing ϕ_c. Thus, the viscosity in both bulk colloidal suspensions and phospholipid monolayers scales, within experimental error, with a power law exponent of 2.

Fig. 5C tests this behavior for spheres diffusing on a 2D membrane. We find a linear scaling between the particle area fraction and their diffusion coefficient of 1.07, which is around a factor of 2 lower than the scaling observed in the bulk suspension and monolayer systems. It is possible that particles tethered to membranes are interacting with each other less strongly than in the other systems, causing η_{app} to increase more slowly with increasing concentration and is consistent with the decrease in diffusion coefficient. In addition, differences in the intrinsic viscosities of the different systems may be a factor in the scaling differences. In the 2D monolayer system, the continuous phase viscosity, η_{so}, was determined to be 0.16 µPa s m, which is three orders of magnitude larger than the viscosity measured in the dilute case for DOPC and indeed much larger than bilayer viscosities reported in literature. Although we have examined a wide range of area fractions and have approximated biological levels of crowding, we are interesting in pursuing these results to higher concentrations, which are more readily accessible in the monolayer and bulk suspension case, in order to probe the limits of the observed scaling and any deviations. In addition, synthetic techniques to control microparticle surface chemistry and strength of interaction with bilayer membranes,[61] or the addition of depletant molecules to the aqueous phase[62] may be applied in the future to manipulate particle–particle interactions and particle–bilayer interactions to study their effects on membrane dynamics.

4 Conclusions

Neutravidin coated particles strongly bound to biotinylated lipids in a bilayer were used as probes to interrogate changes in diffusion dynamics and apparent membrane viscosity as the particle crowding increased. While the membrane viscosity determined using the NLP hydrodynamic model agreed with alternative approaches in the dilute regime, the flexible nature of the bilayer interface contributes to important contrasts to monolayer and bulk systems in crowded environments. As the particles became highly crowded, subdiffusion and non-Gaussian dynamics were observed. Both the scaling in diffusion coefficient and membrane viscosity point towards a decrease in steric effects in the bilayer system. This may have important biological ramifications and explain how membranes are able to maintain their fluidity despite being decorated with high concentrations of integral and peripheral membrane proteins. Careful manipulation of both the membrane biophysical properties through lipid chemistry

and inclusion size in the future is expected to further elucidate the nontrivial interplay between lipids and the dynamics of membrane-bound objects.

Author contributions

Conflicts of interest

There are no conflicts of interest to declare.

Acknowledgements

Notes and references

1 F. Höfling and T. Franosch, *Rep. Prog. Phys.*, 2013, **76**, 046602.
2 B. Alberts, A. Johnson, J. Lewis, M. Raff and K. Roberts, 2007.
3 M. Lindén, P. Sens and R. Phillips, *PLoS Comput. Biol.*, 2012, **8**(3), e1002431.
4 M. Löwe, M. Kalacheva, A. J. Boersma and A. Kedrov, *FEBS J.*, 2020, **287**, 5039–5067.
5 R. Irannejad and M. von Zastrow, *Curr. Opin. Cell Biol.*, 2014, **27**, 109–116.
6 W. T. Snead, C. C. Hayden, A. K. Gadok, C. Zhao, E. M. Lafer, P. Rangamani and J. C. Stachowiak, *Proc. Natl. Acad. Sci. U. S. A.*, 2017, **114**, E3258–E3267.
7 W. T. Snead and J. C. Stachowiak, *J. Mol. Biol.*, 2018, **430**, 2293.
8 A. L. Duncan, T. Reddy, H. Koldsø, J. Hélie, P. W. Fowler, M. Chavent and M. S. Sansom, *Sci. Rep.*, 2017, **7**, 1–15.
9 E. Perozo, A. Kloda, D. M. Cortes and B. Martinac, *Nat. Struct. Biol.*, 2002, **9**, 696–703.
10 M. Weiss, H. Hashimoto and T. Nilsson, *Biophys. J.*, 2003, **84**, 4043–4052.
11 C. Manzo and M. F. Garcia-Parajo, *Rep. Prog. Phys.*, 2015, **5**(1), 011021.
12 A. V. Weigel, M. M. Tamkun and D. Krapf, *Proc. Natl. Acad. Sci. U. S. A.*, 2013, **110**, E4591–E4600.
13 W. He, H. Song, Y. Su, L. Geng, B. J. Ackerson, H. B. Peng and P. Tong, *Nat. Commun.*, 2016, **7**, 1–8.
14 A. V. Weigel, B. Simon, M. M. Tamkun and D. Krapf, *Proc. Natl. Acad. Sci. U. S. A.*, 2011, **108**, 6438–6443.
15 S. Sadegh, J. L. Higgins, P. C. Mannion, M. M. Tamkun and D. Krapf, *Phys. Rev. X*, 2017, **7**, 011031.

16 M. Javanainen, H. Martinez-Seara, R. Metzler and I. Vattulainen, *J. Phys. Chem. Lett.*, 2017, **8**, 4308–4313.

17 J. H. Jeon, M. Javanainen, H. Martinez-Seara, R. Metzler and I. Vattulainen, *Phys. Rev. X*, 2016, **6**, 021006.

18 E. Yamamoto, A. C. Kalli, T. Akimoto, K. Yasuoka and M. S. Sansom, *Sci. Rep.*, 2015, **5**, 1–12.

19 E. Yamamoto, T. Akimoto, A. C. Kalli, K. Yasuoka and M. S. Sansom, *Sci. Adv.*, 2017, **3**(1), e1601871.

20 R. Peters and R. J. Cherry, *Proc. Natl. Acad. Sci. U. S. A.*, 1982, **79**(14), 4317–4321.

21 H. L. Coker, M. R. Cheetham, D. R. Kattnig, Y. J. Wang, S. Garcia-Manyes and M. I. Wallace, *Biophys. J.*, 2019, **116**, 1085–1094.

22 M. R. Horton, F. Höfling, J. O. Rädler and T. Franosch, *Soft Matter*, 2010, **6**, 2648–2656.

23 J. R. Houser, D. J. Busch, D. R. Bell, B. Li, P. Ren and J. C. Stachowiak, *Soft Matter*, 2016, **12**, 2127–2134.

24 S. Ramadurai, A. Holt, V. Krasnikov, G. V. D. Bogaart, J. A. Killian and B. Poolman, *J. Am. Chem. Soc.*, 2009, **131**, 12650–12656.

25 C. C. Lee and N. O. Petersen, *Biophys. J.*, 2003, **84**, 1756–1764.

26 K. WeiÃŸ, A. Neef, Q. Van, S. Kramer, I. Gregor and J. Enderlein, *Biophys. J.*, 2013, **105**, 455–462.

27 P. Saffman and M. Delbruck, *Proc. Natl. Acad. Sci. U. S. A.*, 1975, **72**, 3111–3113.

28 T. T. Hormel, S. Q. Kurihara, M. K. Brennan, M. C. Wozniak and R. Parthasarathy, *Phys. Rev. Lett.*, 2014, **112**, 1–5.

29 P. E. Jahl and R. Parthasarathy, *Biophys. J.*, 2021, **120**, 5513–5520.

30 W. B. Russel, D. A. Saville and W. R. Schowalter, *Colloidal Dispersions*, Cambridge University Press, 1989.

31 J. F. Brady, *J. Chem. Phys.*, 1993, **99**, 567–581.

32 P. Kralchevsky and K. Nagayama, *Particles at Fluid Interfaces and Membranes*, Elsevier Science, 1st edn, 2001.

33 Y. Peng, W. Chen, T. M. Fischer, D. A. Weitz and P. Tong, *J. Fluid Mech.*, 2009, **618**, 243–261.

34 A. K. Sachan, S. Q. Choi, K. H. Kim, Q. Tang, L. Hwang, K. Y. Lee, T. M. Squires and J. A. Zasadzinski, *Soft Matter*, 2017, **13**, 1481–1492.

35 P. J. Beltramo, R. V. Hooghten and J. Vermant, *Soft Matter*, 2016, **12**, 4324–4331.

36 P. J. Beltramo, L. Scheidegger and J. Vermant, *Langmuir*, 2018, **34**, 5880–5888.

37 P. Liu, O. Zabala-Ferrera and P. J. Beltramo, *Biophys. J.*, 2021, **120**, 1755–1764.

38 L. Scheidegger, L. Stricker, P. J. Beltramo and J. Vermant, *J. Phys. Chem. B*, 2022, **126**, 5842–5854.

39 O. Zabala-Ferrera, P. Liu and P. J. Beltramo, *Membranes*, 2023, **13**, 129.

40 J. C. Crocker and D. G. Grier, *J. Colloid Interface Sci.*, 1996, **179**, 298–310.

41 D. S. Martin, M. B. Forstner and J. A. Käs, *Biophys. J.*, 2002, **83**, 2109–2117.

42 V. Sposini, D. Krapf, E. Marinari, R. Sunyer, F. Ritort, F. Taheri, C. Selhuber-Unkel, R. Benelli, M. Weiss, R. Metzler and G. Oshanin, *Commun. Phys.*, 2022, **5**, 1–10.

43 H. Seckler and R. Metzler, *Nat. Commun.*, 2022, **13**, 1–13.

44 Y. Nojima and K. Iwata, *J. Phys. Chem. B*, 2014, **118**, 8631–8641.

45 C. Herold, P. Schwille and E. P. Petrov, *Phys. Rev. Lett.*, 2010, **104**(14), 148102.

46 G. J. Amador, D. van Dijk, R. Kieffer, M.-E. Aubin-Tam and D. Tam, *Proc. Natl. Acad. Sci. U. S. A.*, 2021, **118**(21), e2100156118.

47 Y. Wu, M. Stefl, A. Olzynska, M. Hof, G. Yahioglu, P. Yip, D. R. Casey, O. Ces, J. Humpolickova and M. K. Kuimova, Molecular rheometry: direct determination of viscosity in L_o and L_d lipid phases *via* fluorescence lifetime imaging, *Phys. Chem. Chem. Phys.*, 2013, **15**, 14986–14993.

48 H. A. Faizi, R. Dimova and P. M. Vlahovska, *Biophys. J.*, 2022, **121**, 910–918.

49 S. Chakraborty, M. Doktorova, T. R. Molugu, F. A. Heberle, H. L. Scott, B. Dzikovski, M. Nagao, L.-R. Stingaciu, R. F. Standaert, F. N. Barrera, J. Katsaras, G. Khelashvili, M. F. Brown and R. Ashkar, *Proc. Natl. Acad. Sci. U. S. A.*, 2020, **117**, 21896–21905.

50 B. D. Hughes, B. A. Pailthorpe and L. R. White, *J. Fluid Mech.*, 1981, **110**, 349–372.

51 E. P. Petrov, R. Petrosyan and P. Schwille, *Soft Matter*, 2012, **8**, 7552–7555.

52 A. Naji, A. J. Levine and P. A. Pincus, *Biophys. J.*, 2007, **93**, 49–51.

53 X. Qiu, X. L. Wu, J. Z. Xue, D. J. Pine, D. A. Weitz and P. M. Chaikin, *Phys. Rev. Lett.*, 1990, **65**, 516–519.

54 W. van Megen, S. M. Underwood, R. H. Ottewill, N. J. S. Williams and P. N. Pusey, *Faraday Discuss. Chem. Soc.*, 1987, **83**, 47–57.

55 F. Hofling and T. Franosch, *Rep. Prog. Phys.*, 2013, **76**, 50.

56 M. J. Saxton, *Biophys. J.*, 1994, **66**, 394–401.

57 I. Y. Wong, M. L. Gardel, D. R. Reichman, E. R. Weeks, M. T. Valentine, A. R. Bausch and D. A. Weitz, *Phys. Rev. Lett.*, 2004, **92**, 30–33.

58 J. Hyung Jeon, H. M. Seara Monne, M. Javanainen and R. Metzler, *Phys. Rev. Lett.*, 2012, **109**, 188103.

59 K. Speckner and M. Weiss, *Entropy*, 2021, **23**, 892.

60 P. S. Niemelä, M. S. Miettinen, L. Monticelli, H. Hammaren, P. Bjelkmar, T. Murtola, E. Lindahl and I. Vattulainen, *J. Am. Chem. Soc.*, 2010, **132**, 7574–7575.

61 C. V. D. Wel, N. Bossert, Q. J. Mank, M. G. Winter, D. Heinrich and D. J. Kraft, *Langmuir*, 2017, **33**, 9803–9810.

62 H. T. Spanke, J. Agudo-Canalejo, D. Tran, R. W. Style and E. R. Dufresne, *Phys. Rev. Res.*, 2022, **4**, 023080.